ANL-7007

Argonne National Laboratory

PHYSICS MEASUREMENTS IN TUNGSTEN-BASED, ALUMINUM-REFLECTED FAST REACTORS

by

R. C. Doerner, W. G. Knapp,
K. K. Almenas, and R. A. Karam

DISCLAIMER

The facilities of Argonne National Laboratory are owned by the United States Government. Under the terms of a contract (W-31-109-Eng-38) between the U. S. Atomic Energy Commission, Argonne Universities Association and The University of Chicago, the University employs the staff and operates the Laboratory in accordance with policies and programs formulated, approved and reviewed by the Association.

MEMBERS OF ARGONNE UNIVERSITIES ASSOCIATION

The University of Arizona
Carnegie Institute of Technology
Case Institute of Technology
The University of Chicago
University of Cincinnati
Illinois Institute of Technology
University of Illinois
Indiana University
Iowa State University
The University of Iowa
Kansas State University
The University of Kansas
Loyola University
Marquette University
Michigan State University
The University of Michigan
University of Minnesota
University of Missouri
Northwestern University
University of Notre Dame
The Ohio State University
Purdue University
Saint Louis University
Washington University
Wayne State University
The University of Wisconsin

Printed in the United States of America
Available from
Clearinghouse for Federal Scientific and Technical Information
National Bureau of Standards, U. S. Department of Commerce
Springfield, Virginia 22151
Price: Printed Copy $3.00; Microfiche $0.65

ANL-7007
Reactor Technology
(TID-4500)
AEC Research and
Development Report

ARGONNE NATIONAL LABORATORY
9700 South Cass Avenue
Argonne, Illinois 60439

PHYSICS MEASUREMENTS IN TUNGSTEN-BASED, ALUMINUM-REFLECTED FAST REACTORS

by

R. C. Doerner, W. G. Knapp,
K. K. Almenas, and R. A. Karam

Reactor Physics Division

March 1967

TABLE OF CONTENTS

LIST OF FIGURES

LIST OF TABLES

PHYSICS MEASUREMENTS IN TUNGSTEN-BASED, ALUMINUM-REFLECTED FAST REACTORS

by

R. C. Doerner, W. G. Knapp,
K. K. Almenas, and R. A. Karam

I. INTRODUCTION

An experimental physics-neutronics study of materials and design concepts for proposed high-temperature fast reactors has been undertaken in support of the Argonne National Laboratory rocket-design effort. In the basic design, the fuel is highly enriched U^{235}, the major diluent is a tungsten-rhenium alloy, and the reflector material is a light metal or metal oxide. Initial studies have concerned specifically tungsten as a diluent in moderate-volume (100- to 300-liter) fast-reactor cores and aluminum as the reflector. This report summarizes the results of measurements made on four fast critical experiments performed in ZPR-9. A major objective of these experiments was to provide the necessary data for selection of a single, multigroup, tungsten cross-section set from the several generated for this program.

A suitable reference for these studies is the depleted-uranium-diluted and -reflected reactor[1] first constructed as ZPR-3 Assembly No. 11. Subsequently, it was reconstructed as ZPR-3 Assembly No. 22 and ZPR-6 Assembly No. 1. The core U^{238}-to-U^{235} ratio was 7:1, and the reactor construction material (matrix and fuel drawers) was stainless steel.

ZPR-9, a counterpart of ZPR-6,[2] except that the ZPR-9 matrix and fuel drawers are aluminum, was used for these studies. Four fast-reactor assemblies were constructed as part of this program.

The first core studied (Assembly No. 1) was the standard 7:1 volume ratio of U^{238} to U^{235}, which differed from the reference assembly only in the use of aluminum as the reflector and matrix structure material rather than a depleted-uranium reflector and a stainless matrix. These studies were of particular interest in evaluating the effects of aluminum as a reflector material in comparison with the better-known depleted-uranium reflector.

In subsequent reactor assemblies, one-fourth, one-half, and all of the U^{238} diluent were homogeneously replaced by tungsten. The compositions of these assemblies are given in Table VI. In Assembly No. 4, lengthening of the core and increased fuel concentration were necessary to achieve a realistic core configuration as tungsten was added.

Standard techniques were used in the measurement of critical geometry, Rossi-alpha, and central fuel and material worths so that trends could be detected. These could then be compared with trends in the calculated model as a function of varying tungsten content and other core-parameter variations. In addition to these measurements, a limited number of central-worth measurements were made on boron and hydrogenous samples to evaluate the effect of sample size. In Assembly No. 4, the central-worth measurements of aluminum, rhenium, carbon, and tungsten were augmented by measurements of the spatially dependent worth of these materials in the aluminum reflector.

II. DESCRIPTION OF THE CRITICAL REACTOR ASSEMBLIES

ZPR-9 is a split-table-type, fast-reactor critical facility, as shown in Fig. 1. Fuel and diluent material in the form of metal plates, color-coded for easy identification, were loaded into drawers with a 2 x 2 cross section. Core lengths could be readily varied in increments of 1 or 2 in. Both axial and radial aluminum metal reflector material was used, the axial reflector material being partially loaded in the fuel drawer and partially in a back drawer. In all cases, the reflector was 30-35 cm thick.

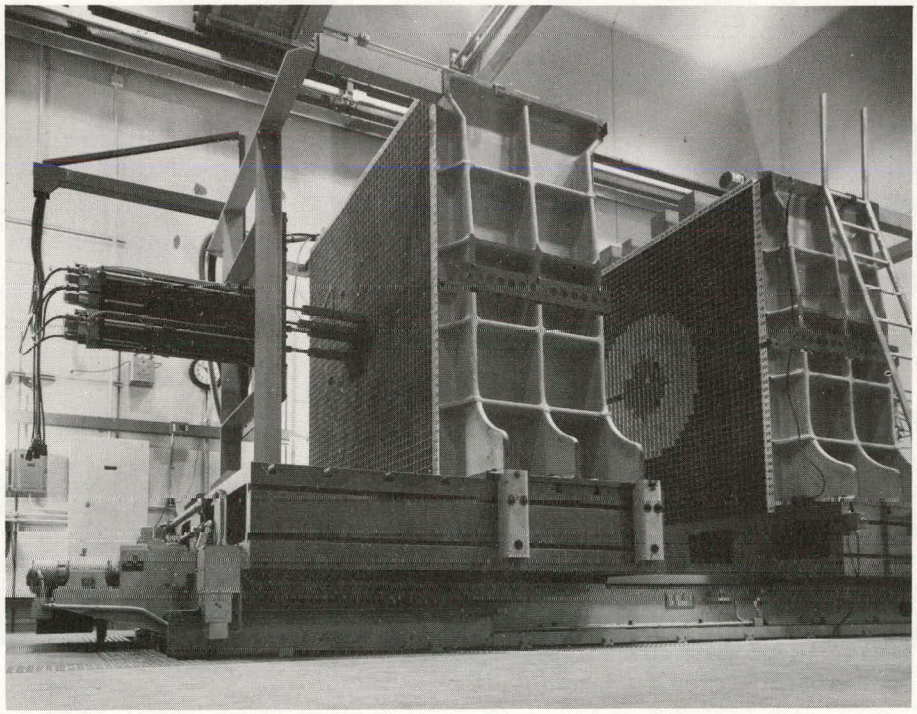

112-3627

Fig. 1. ZPPR-9 Fast Critical Assembly

A. Assembly No. 1

Assembly No. 1 was intended to be a close copy of the reference assembly except for the use of aluminum both for reactor structure and for the reflector material. Two 1/8-in.-thick by 10-in.-long columns of enriched uranium were loaded with fourteen 1/8-in. columns of depleted uranium in each drawer so that the core had an even distribution of fuel and diluent material.

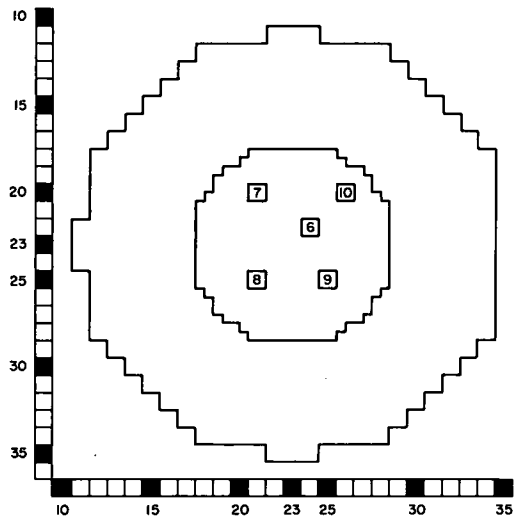

112-7918

Fig. 2. Geometric Outline of Assembly No. 1 Loading 9

The order of fuel (F) and diluent (depleted uranium, D) in a drawer in the core was DDDFDDDDDDDFDDDD. Each column of material was made up of 2 x 2-in. and 2 x 3-in. pieces, placed end-to-end, forming 10-in.-long columns in the drawers. The fuel pieces throughout the studies reported here were 1/8-in.-thick, 93.2% enriched U^{235}. The depleted uranium pieces were also 1/8 in. thick and were 99.8% U^{238}. An outline of a reasonably circular and symmetric critical loading (Loading No. 9) is shown in Fig. 2. The fuel inventory, including the U^{235} content of the diluent, was 282.71 kg of U^{235}. The excess reactivity of this loading was 86.8 Ih. Full or partially filled drawers were added or removed from the core periphery in subsequent loadings, giving a nearly cylindrical core boundary. The edge worth of fuel material was determined at this time. Including an estimated 0.75-mm air gap at the core midplane and the thickness of the aluminum drawer fronts, the effective core length of Assembly No. 1 is 51.04 cm. These data are summarized in Table I.

TABLE I. Properties of ZPR-9 Assemblies No. 1 through 4

	Assembly No. 1 Loading 9	Assembly No. 2 Loading 13	Assembly No. 3 Loading 10	Assembly No. 4 Loading 10	Reference Assembly[a]
As-loaded mass,[b] kg U^{235}	282.71	394.12	501.46	287.57	232.29
Core radius, cm	31.58	34.11	35.79	25.21	28.47
Outer reflector radius, cm	66.64	70.28	70.28	65.37	65.34
Excess reactivity, Ih	86.8	165.0	103.1	75.1	51.4
Core length, cm[c]	51.04	61.20	71.36	56.12	51.04
Fuel-edge worth, Ih/kg	24.7	18.8	12.1	31.9	27.7
Critical mass,[d] kg U^{235}	279.2	385.3	492.9	285.2	230.4

[a]ZPR-6 Assembly No. 1 (loading 8).
[b]Does not include U^{235} in the depleted uranium diluent.
[c]Includes 1.68 mm for the aluminum drawer fronts plus 0.75-mm air gap in the core midplane.
[d]Corrected for excess reactivity only.

The critical mass of an assembly is determined by subtracting from the total fuel inventory in the core (kg of U^{235}) a quantity of fuel equivalent to the total excess reactivity of a given loading in terms of peripheral fuel.

B. Assembly No. 2

At the end of Assembly No. 1 studies, the core drawers were replaced, an octant at a time, with drawers having two columns of fuel, ten columns of depleted uranium, and four columns of tungsten, all 1/8 in. wide and 12 in. long. In the notations used above, the arrangement of pieces was DWDFDWDDDWDFDWDD, where W represents columns of tungsten. Each octant was loaded until the system was critical. Since none of the octants included the central drawers, these were loaded separately and provided a measure of the central fuel worth. After each loading, the total excess reactivity was determined by a previously calibrated rod located in the last octant to be loaded. Results of this loading procedure indicated that reactivity effects associated with the change in composition added in an approximately linear manner for the various regions.

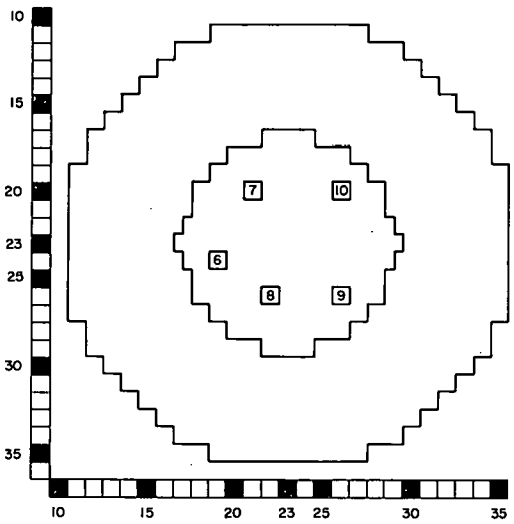

112-7917

Fig. 3. Geometric Outline of Assembly No. 2 Loading 13

As the core became larger, the worth of this rod decreased. This change in worth was not taken into account in the reactivity inventory during the loading procedure. In Assembly No. 1 this rod had an integral worth of 141 Ih; in Assembly No. 2 it was worth 126 Ih. Also not considered was the changing relation between reactivity and period as the geometry and core composition changed.

A geometric outline of loading 13 is shown in Fig. 3, and the various critical properties of Assembly No. 2 are listed in Table I.

C. Assembly No. 3

In the third assembly of this series, seven columns, or half of the original depleted-uranium diluent material, were replaced by tungsten. Drawers were loaded with 14-in.-long columns of materials in the sequence DWDFWDWDWDWFDWDW. The geometric outline of one of the critical loadings (No. 10) is shown in Fig. 4, and the critical properties are listed in Table I.

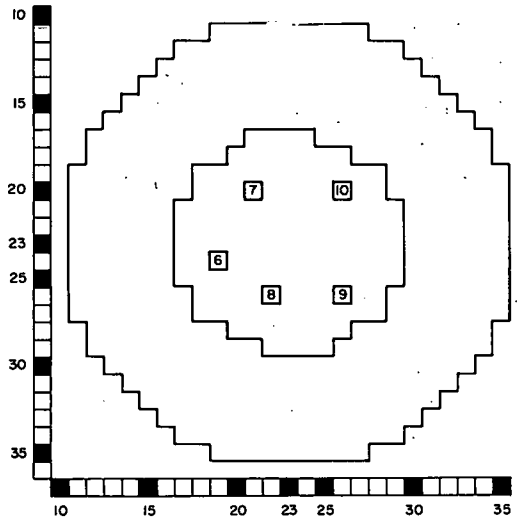

112-7916

Fig. 4. Geometric Outline of Assembly No. 3 Loading 10

D. Assembly No. 4

Assembly No. 4, an all-tungsten-diluted core with an aluminum reflector, marked the logical termination of the first series of experiments in which the neutronic properties of tungsten were systematically studied relative to the comparable properties of depleted uranium. It also provided a reference of comparison for further studies in tungsten-rhenium-, tungsten-graphite-, and tungsten-aluminum-diluted systems and was, therefore, the most extensively studied of all the ZPR-9 assemblies.

Because of a limited supply of tungsten material, the fuel density was increased 50% relative to the previous assemblies. Also, 1/16-in.-thick fuel plates were made available for this assembly, allowing a more nearly homogeneous loading and consequently a smaller correction for heterogeneity effects. Drawers were loaded with 11-in.-long columns of 1/8-in. tungsten with uniformly distributed 1/16-in. fuel columns (f) in the sequence WfWWfWWfWWfWWfWWfWW. The geometric and neutronic properties of this loading are given in Fig. 5 and Table I, respectively.

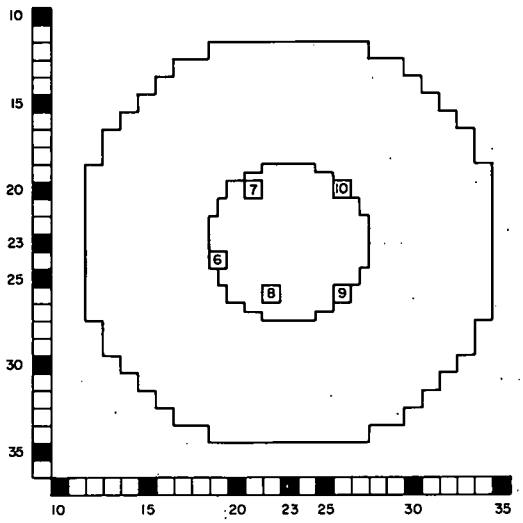

112-7915

Fig. 5
Geometric Outline of Assembly No. 4 Loading 10

E. Summary of ZPR-9 Assembly Compositions

The physical properties of the first four assemblies are summarized in Table I. Included are the corresponding properties of the reference assembly. Except as noted in this and subsequent tables, the quoted values for the reference assembly apply to ZPR-6 Assembly No. 1.

III. EXPERIMENTAL RESULTS AND THEIR INTERPRETATION

Although most of the measurable parameters can be determined with good accuracy, their interpretation in terms of the basic physics parameters is by no means simple. Ultimate accuracy in most experimental measurements is limited by the precision with which an experimental reactivity effect can be measured. Experience has shown that this limit is approximately ±0.02 Ih and has its origin in pile and instrument noise as well as human and instrument bias. Cross sections, on the other hand, are known to perhaps ±5%, so that calculated values of the critical mass, central worths, reaction rates, etc., have uncertainties associated with them. Then, too, differences between measured and calculated values will depend, at least in part, on the calculational model chosen.

With few exceptions, all calculations in connection with this program were made using one-dimensional, 16-group, diffusion-theory codes in spherical or cylindrical geometry as required or available. The experimental cores were fully reflected, cylindrical assemblies with L/D ratios between 0.8 and 1.2.

A. Critical Mass

In all cases, corrections for the heterogeneity effects of the moderately thick fuel columns, the central gap characteristic of split-bed-type machines, and the irregularity of the pseudocylindrical boundary of the experimental geometry were made in terms of the required amount of peripheral fuel that must be removed or added to exactly compensate for the reactivity involved in each effect. The accuracy with which any corrections were made was determined directly by the accuracy with which the fuel-edge worth had been determined. These corrections are summarized in Table II and are discussed in the paragraphs below.

1. Fuel-edge Worth and Experimental Critical Mass

Several factors contribute to the uncertainty of the fuel-edge worth values as listed in Table II, which may be of the order of 5 to 10%. These include variations and/or uncertainties in control-rod worth, control-rod positions at critical, and fuel inventory per drawer. The latter effect is brought about by the frequent necessity to use different size pieces from drawer to drawer in order to obtain the necessary loading with the fuel available. Lesser effects associated with changes in radial buckling and core boundary as fuel is added or removed during the experiment also contribute to the uncertainty in the measurement.

TABLE II. Comparison of Experimental and Critical Masses

	ZPR-6 Assembly No. 1, Reference Assembly		ZPR-9							
			Assembly No. 1		Assembly No. 2		Assembly No. 3		Assembly No. 4	
	Exp	Calc	Exp	Calc	Exp	Calc	Exp	Calc	Exp	Calc
Inhours/% $\Delta k/k$		477		469		457		446		430
Fuel-edge worth	27.7		24.65	20.8	18.76	15.7	12.11	12.3	31.87	27.6
(E - C)/C				0.18		0.19		0.01		0.15
$(\Delta M/M)/(\Delta k/k)$	7.14	7.2	6.09	8.1	7.20	7.6	7.01	7.4	4.67	5.46
U^{235} Mass loaded	232		283		394		501		288	
Excess reactivity, Ih	51.4		86.77		165		103.06		75.10	
kg U^{235}	1.85		3.52		8.79		8.51		2.36	
Experimental critical mass, kg U^{235}	230		279		385		493		285	
Heterog corr, % $\Delta k/k$	+0.76		+0.82		+0.86		+0.91		+0.30	
kg U^{235}	+13.09		+15.60		+20.94		+33.51		+4.05	
Central gap, % $\Delta k/k$	-0.031		-0.031		-0.031		-0.031		-0.031	
kg U^{235}	-0.53		-0.59		-0.76		-1.14		-0.42	
Irregular edge, % $\Delta k/k$	-0.02		-0.02		-0.02		-0.02		-0.02	
kg U^{235}	-0.36		-0.38		-0.48		-0.74		-0.27	
EHCCM,[a] kg U^{235}	243		294		405		525		289	
Shape factor	0.937		0.938		0.936		0.916		0.931	
EHSCM[b] exp, kg U^{235}	227		276		379		481		269	
EHSCR,[c] cm	31.2		34.1		37.2		40.4		29.0	
EHSCV,[d] liters	127		165		215		275		102	

[a]Equivalent homogeneous cylindrical critical mass.
[b]Equivalent homogeneous spherical critical mass.
[c]Equivalent homogeneous spherical critical radius.
[d]Equivalent homogeneous spherical critical volume.

The calculated values listed in Table II were determined from a one-dimensional, 16-group, diffusion-theory code in which the atom densities were fixed by the experiment and k was calculated for two different-radii cylindrical cores, both close to the experimental radius. In one-dimensional calculations in cylindrical geometry, the calculational model could only assume an absence of axial reflector material. To correlate the calculational model with the experimental model at the radial midplane for edge-worth and reaction-rate computations, it was necessary to modify the core absorption so as to simulate neutron leakage from the ends of the core. This was accomplished by using a very long (1000-cm) core and reflector, with a synthetic absorber with group cross sections calculated from the leakage out divided by the flux integral for each group taken from a comparable spherical problem.

Since the calculated $(\Delta M/M)/(\Delta k/k)$ is based on a homogeneous fuel distribution, the experimental values were derived from critical masses corrected for heterogeneity, central gap, and boundary irregularities (EHCCM in Table II).

2. Heterogeneity

The magnitude of the correction for fuel-plate heterogeneity was determined by fuel "bunching" experiments, i.e., by determining the reactivity effect of combining two or more columns of fuel into a single column. The effect of heterogeneity is to make the experimental core smaller. The correction is made to the critical mass by adding an amount of edge core material equivalent to the reactivity effect of the fuel heterogeneity.

Depending on the absorption cross sections of the diluent materials, there may also be neutron streaming between the thick fuel columns. The aluminum matrix and drawer sides provide a low absorption path for neutron streaming, but the dimensions are small relative to λ_{tr} and the effect is expected to be small.

To determine the magnitude of the heterogeneity correction (including streaming effects), fuel from two octants of Assembly No. 4 was bunched to produce the configurations indicated in Table III. Assuming a linear scaling factor between the octant measurement and full core conditions gave the corrections indicated in Table III. Similar measurements reported for the reference cores are also included. These corrections are plotted in Fig. 6, the scale to the left being relative to the 1/16-in. fuel columns, the scale to the right being the absolute correction based on a reasonable extrapolation of the measured data to infinite dilution conditions. Thus, the heterogeneity correction for Assembly No. 4 using 1/16-in.-thick fuel plates is +0.3% $\Delta k/k$. For Assembly No. 1 (the same core composition as the reference assemblies), the correction was chosen as the average of the two reference assemblies studied: +0.82%. Intermediate values for the heterogeneity corrections for Assemblies No. 2 and 3 were chosen on the basis of their U^{238}-to-tungsten volume ratios. The magnitude of the assumed correction for each assembly is given in Table II.

TABLE III. Fuel-bunching Results in $\Delta k/k$ Relative to 1/16-in.-thick Fuel Columns

Fuel Thickness, cm	No. of Fuel Columns per Drawer	Center-to-Center Spacing between Fuel Columns, cm	Reactivity Added		
			ZPR-9 Assembly No. 4	ZPR-6[a] Assembly No. 1	ZPR-3[b] Assembly No. 22
0.159	6	0.922	0		
0.159	4	1.383		0	0
0.318	3	1.843	+0.66%		
0.318	2	2.765		+0.44%	+0.4%
0.477	2	2.765	+2.06%		
0.635	1	5.530		+1.23%	+1.3%

[a]Communicated by W. Y. Kato, Argonne National Laboratory.
[b]Communicated by D. Meneghetti, Argonne National Laboratory.

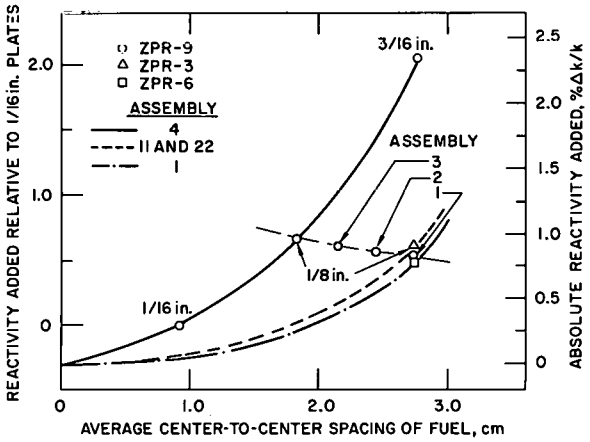

112-7919

Fig. 6. Heterogeneity Corrections for Assemblies No. 1 through 4

3. Central Gap

In addition to the thickness of the aluminum drawer fronts (0.084 cm per drawer), an air gap, estimated to average 0.076 cm, exists. To estimate the correction for this gap, the worths of gaps up to 2 mm wide were measured in Assembly No. 4 and extrapolated to a point 2 mm beyond the indicated zero table separation. The measured data and its extrapolation are shown in Fig. 7, the left scale being the gap worth relative to indicated table separation, the right scale being the estimated absolute worth. A similar measurement on the reference core[3] (ZPR-6 Assembly No. 1) is also shown, but because of the detector location (very close to the gap where streaming may also affect the results), the gap correction is probably overestimated. However, the estimated correction for ZPR-3 Assembly No. 11 is even higher[1] (0.18% $\Delta k/k$) than the ZPR-6 data (0.10% $\Delta k/k$).

The fact that nearly 70% of the existing gap is aluminum, while the extrapolation to zero gap is based on measurements with air, further complicates this correction. Nevertheless, all the ZPR-9 assemblies have been assigned (somewhat arbitrarily) a -0.02% $\Delta k/k$ correction for the central gap. This corresponds to a 2.43-mm central gap; 0.76 mm for air, plus 1.67 mm for the aluminum drawer fronts. This correction, in terms of the critical mass, is shown in Table II.

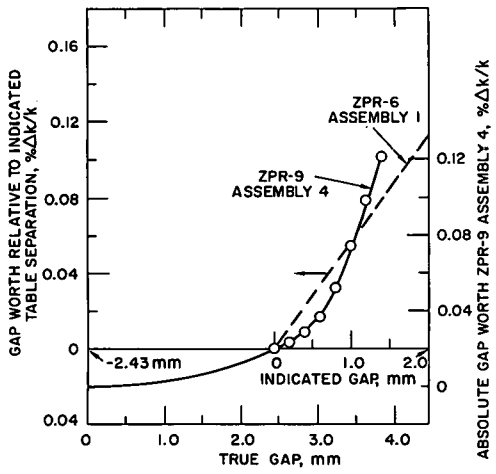

112-7920

Fig. 7. Central Gap Worth of Assembly No. 4

4. Edge Effects

A small correction must be made for the increased leakage from the irregularly bounded pseudocylinder of the experimental geometry relative to the equivalent smooth surface assumed in the calculations. From studies on ZPR-3 (Ref. 4), this correction is estimated as -0.02% $\Delta k/k$.

5. Shape Factor

A two-step shape factor, as reported by Davey,[4] is used to convert the experimental homogeneous critical mass determined in cylindrical

geometry to the equivalent spherical critical mass. After the experimental critical mass has been corrected for heterogeneity, central gap, and irregular edge effects, the core volume and equivalent spherical radius are determined (see Table II). The shape factors, as given by Davey, consist of the product of a volume-dependent term and a term dependent on the cylindrical core length-to-diameter ratio. They are given for each ZPR-9 assembly in Table II.

6. Calculated Critical Mass

Calculating procedures were standardized for all assemblies in an effort to study trends in the experimental data without the influence of varying calculation methods or cross-section sets. All routine calculations were performed by the multigroup, single-dimension, diffusion-theory code (RP-122). A few calculations were performed with the multigroup transport-theory code (DSN) for the purpose of evaluating limitations of the diffusion theory in calculating these assemblies. A series of five tungsten cross-section sets, each having 16 groups, was generated from different input data and different group-averaging procedures. Before the experimental critical program, the effects of these differences were extensively studied. The one set that consistently gave the best agreement between theory and experiment is given in the appendix.

7. Comparison of Experimental to Calculated Mass

The basic analytical "package" employed for interpreting the experimental results has been the ANL cross-section Set 201[13,17] (including its various options for tungsten) in conjunction with one-dimensional diffusion or transport codes, both in spherical and cylindrical geometry. Because of machine-time economics, the RP-122 diffusion code has been used most frequently. Results are summarized and compared to experimental values in Table IV.

The differences between the calculated and experimental results, both in terms of critical mass and in terms of reactivity, are given in the last rows of Table IV. The differences shown are simply those between experiment and calculation obtained using a specific method of analysis and do not represent the "uncertainty" of analytical critical-mass methods in general. Without changing the input data or the code, and by employing a different mode of convergence (calculating the critical concentration instead of the critical radius), the absolute value of the difference is reduced considerably. This is especially true for the assemblies reported here, since the relatively poor reflective properties of aluminum give the assemblies a low fuel-edge worth. Consequently, a critical radius calculation will strongly amplify any reactivity-dependent errors. The true "uncertainty" is reduced further by the fact that several of the error sources contributing to this overall difference have been identified previously and can be corrected for. This includes the errors due to U^{238} cross-section sets used and those due

to the diffusion-theory approximation. Transport methods such as the DSN code reduce the absolute values of the errors by approximately 50%. Table V gives a probable breakdown of the major error sources. As shown, no consistent, systematic error is attributed to the tungsten cross-section sets. The interpretation is as follows: Based on the critical-mass measurements of Assemblies No. 2 to 4, the theory-to-experiment discrepancy that could be attributed to the tungsten cross-section sets is smaller than other identified discrepancies for these assemblies. Therefore errors in the tungsten cross-section sets probably introduce less than a 3% error in critical mass or less than 0.005 in terms of Δk. Measurements of central material worths support this conclusion. The contribution of a large number of factors to a critical mass calculation makes it difficult--if not impossible--to identify and evaluate the influence of separate components except within fairly broad limits.

TABLE IV. Assembly Compositions

	ZPR-6	ZPR-9			
	Assembly No. 1	Assembly No. 1	Assembly No. 2	Assembly No. 3	Assembly No. 4
Heterogeneous critical component[a]					
U^{235} kg	230	279	385	493	285
U^{235} v/o	9.9	9.6	9.6	9.7	14.5
U^{235} atom density	0.00453	0.00454	0.00452	0.00448	0.00677
U^{238} kg	1788	2110	2151	1899	21
U^{238} v/o	73.1	72.7	53.4	37.3	1.1
U^{238} atom density	0.0338	0.0338	0.0243	0.0170	0.000483
Al kg		47.1	66.8	84.6	32.6
Al v/o		11.3	11.3	11.3	11.3
Al atom density		0.00665	0.00666	0.00667	0.00665
Fe kg	98.3	7.7	9.2	10.8	8.5
Fe v/o	9.7	0.64	0.54	0.50	1.02
Fe atom density	0.00939	0.000526	0.000412	0.000411	0.000837
W kg			835	1849	1142
W v/o			20.9	36.6	58.6
W atom density			0.0122	0.0214	0.0341
Void v/o	7.3	5.7	4.3	4.5	13.6
EHSCM[b]	227	276	379	481	269
EHSCV[c]	127	156	215	275	102
Calculated critical mass[d]	289	325	452	543	305
Calculated critical volume	164	184	263	312	117
Radius	33.9	35.3	39.7	42.1	30.3
ΔM	61.9	49.6	72.5	62.6	35.9
(E - C)/C in mass	-0.21	-0.15	-0.17	-0.11	-0.12
(E - C)/C in k_{eff}[e]	-0.036	-0.026	-0.030	-0.017	-0.027

[a] In units of 10^{24} atoms/cm^3. Experimental value corrected for excess reactivity only.
[b] Equivalent homogeneous spherical critical mass, in kg of U^{235}.
[c] Equivalent homogeneous spherical critical volume, in liters.
[d] RP-122 programmed for the CDC-3600 computer is the MAIM-6 program, and tungsten material 37 in the 201 cross-section library is material 30 in the MAIM-6 library.
[e] Inferred from measured edge worths given in Table II.

TABLE V. Probable Cause of Calculated Reactivity Deviations, in Units of $\Delta k/k$

Assembly	Error due to Limitations of Diffusion Theory	Error due to U^{238} Cross Sections	Error due to Aluminum Cross Sections	Error due to Tungsten (Material No. 37) Cross Sections
ZPR-3 Assembly No. 22	~-0.012	~-0.0075	-	-
ZPR-9 Assembly No. 1	~-0.014	~-0.007	~-0.006	-
ZPR-9 Assembly No. 2	~-0.013	~-0.005	~-0.006	~-0.0007
ZPR-9 Assembly No. 3	~-0.011	~-0.003	~-0.0045	~-0.003
ZPR-9 Assembly No. 4	~-0.014	-	~-0.010	~+0.004

A recently generated 22-group cross-section library (ANL Set 224) was used in recalculating the critical masses of the ZPR-9 assemblies. The purpose of the calculations was to provide a direct comparison of the cross-section libraries, 201 and 224; therefore, the calculations were performed in a comparable manner as for those outlined in Table V. ANL 224 cross-section library has several options for a number of materials; the material numbers employed in this calculation were: U^{238}, U^{235}, iron, aluminum (ELMOE corrected), and tungsten. Results for both sets of calculations are shown in Table VI.

TABLE VI. Comparison of Critical Masses Calculated by Using ANL Cross-section Sets 201 and 224 with Experimental Values

	ZPR-3	ZPR-9			
	Assembly No. 22	Assembly No. 1	Assembly No. 2	Assembly No. 3	Assembly No. 4
EHSCM,[a] kg	239	276	379	481	269
Set 201					
Calculated critical mass, kg	278	332	441	562	294
(E - C)/C critical mass	-0.140	-0.169	-0.140	-0.145	-0.086
k_{eff} (calc) - 1.0[b]	0.0226	0.0295	0.0254	0.0221	0.0187
Set 224					
Calculated critical mass, kg	264	325	452	615	304
(E - C)/C critical mass	-0.095	-0.151	-0.161	-0.619	-0.116
k_{eff} (calc) - 1.0	0.0154	0.0258	0.0299	0.0365	0.0261
Comparison of 201 with 224					
$\frac{CM(224) - CM(201)}{CM(224)}$	-0.05	-0.02	+0.02	+0.087	+0.03
$k_{eff}^{(201)} - k_{eff}^{(224)}$	-0.0072	-0.0037	+0.0045	+0.0144	+0.0074

[a]Experimental homogeneous spherical critical mass.
[b]Calculated k_{eff} value is inferred from fuel-edge worth measurements.

Except for the ZPR-3 Assembly No. 22 (the same as ZPR-6 Assembly No. 1), no marked improvement in calculational agreement can be claimed by the ANL 224 cross sections. A qualitative interpretation of these results is as follows: the ANL 224 cross-section library has a "better" U^{238} cross-section set and not as "good" a tungsten set as the ANL 201 cross-section library. The aluminum set is to be improved.

B. Measurements of Central Reactivity

A distinction is made between worth measurements made with standard nonhydrogenous samples for the purpose of evaluating neutronic properties of the samples, and those made with hydrogenous samples that ultimately relate to propellant and control studies in the rocket reactor. Many standard samples were available for central-worth measurements, all with a nominal outside dimension of 2 x 2 x 1 in. Powdered samples were sealed in welded aluminum or stainless steel cans, except the B^{10} sample, which was contained in a double stainless steel can.

1. Experimental Techniques

In Assemblies No. 1 to 3, samples were manually inserted in a void space at the core center. Each measurement required bringing the reactor halves together. Measurements on clad samples were accompanied by similar measurements using an empty can as a reference. Experience has shown that reproducibility of the reference measurement was generally uncertain by less than 0.5 Ih. Most of this uncertainty was due to inexact reproducibility of table-separation gap and rod in-limit positions. A remote-controlled automatic sample changer was used on Assembly No. 4. With this sample changer, up to 12 samples or reference cans could be measured without separating the table halves or moving the dual-purpose safety rods. Errors associated with these measurements are generally less than 0.07 Ih, a large part of this being due to uncertainties in establishing, in a reasonable period of time, the exact rod position for which the reactor is critical.

2. Calculated Central Reactivities

Calculated values for the central-worth coefficients were obtained by a perturbation-theory computation with unperturbed central real and adjoint fluxes from a 16-group, one-dimensional (spherical) theory calculation. Absolute values for the reactivity were determined from

$$\frac{\Delta k}{k} = -\frac{\sum_{j=1}^{J} \phi_j^* \phi_j \sigma_{rem} - \sum_{j=1}^{J} \sum_{k=1}^{j} \phi_j^* \phi_k \sigma_{k \to j} - \left[\sum_{j=1}^{J} \chi_j \phi_j^*\right]\left[\sum_{j=1}^{J} (\nu\sigma_f)_j \phi_j\right]}{\int_V \left[\sum_{j=1}^{J} (\nu\Sigma_f)_j \phi_j\right]\left[\sum_{j=1}^{J^4} \chi_j \phi_j^*\right] dV},$$

where the symbols have their usual meaning and the denominator is an integration over the core volume. To perform the integration, the ESHCM parameters must be used. Consequently, the calculations were made after the experimental critical mass and atom concentrations had been experimentally determined. The denominator is one term (DCNF) of the output of a reactor kinetics code used to calculate the effective delayed fraction and the prompt-neutron lifetime.

3. Comparison of Experimental and Calculated Central Reactivities

Table VII lists the measured and calculated central worths of the various samples. In most cases the tungsten central worth can be predicted to a higher degree of accuracy than the U^{238} central worth. This is especially true in the cores having large volume fractions of tungsten. The fact that the U^{238} worths are predicted to be more negative by 15-25% than the experimental values indicates an underestimate of the fission and/or an overestimate of the absorption in this material. The same uncertainty is reflected in the comparisons of the experimental to the calculated equivalent spherical homogeneous critical mass listed in Table IV for the reference assembly. The excellence of the predictions for B^{10} is not surprising since the spectra are moderately hard with respect to the boron cross section. The experimental values quoted for hydrogen have been extrapolated to zero sample size corresponding to the infinitely dilute calculation.

TABLE VII. Measured and Calculated Central Reactivities in Ih/kg of Material

	Reference Assembly		ZPR-9							
			Assembly No. 1		Assembly No. 2		Assembly No. 3		Assembly No. 4	
Material	Meas	Calc	Meas	Calc	Meas	Calc	Meas	Calc	Meas	Calc
U^{235}	270	265	250	252	219	216	162	165	270	286
U^{238}	-11.7	-13.5	-10.7	-13	-9.2	-10.8	-6.3	-8.4	-5.5	-7.5
W	-24	-27.3	-21.8	-26.7	-16.7	-21.3	-14.8	-15.6	-19.6	-22.3
WO_2		-21.4	-23.4						-12.6	-13.5
Re	-64.3	-79.5	-57.9	-84.9	-49.9	-74.9	-44.3	-59	-71.7	-110
C	-27.3		-34.8	+12			-21.1	-9.9	-2.5	+59.6
B^{10}	-2760	-2755	-2722	-2934	-2382	-2659	-2110	-2165	-3664	-3835
B_4C									-399.2	-492
H							-350	-2716	+3350	+3494
Al	+18.4	-11.9							-6.6	+8
Al_2O_3									-5.3	+21.8
Zr	-27.3								-5.0	-28.4
ZrH_4									+60	+120
Au			-32.7		-27.3		-23.4		-39.3	
O[a]			-19.1	-4.45					+26.6	+37.5

[a]Determined from the difference between tungsten metal and tungsten oxide.

From the differences between measurements with tungsten and its oxide, and aluminum and its oxide, a value of the central worth for oxygen can be determined. The general experience with these and other tungsten-containing assemblies indicates that the central oxygen worth is generally better predicted from differences between the heavy metals and their oxides (e.g., tungsten) than from the light elements (e.g., aluminum). For this reason, the listed experimental values for oxygen were determined from the measured differences between tungsten and its oxide in both Assemblies No. 1 and 4.

A study of the central-worth data in Assembly No. 4 would indicate that the calculated real-flux spectrum is reasonably accurate while the

large differences and even the change in sign for the elastic and inelastic scattering materials in Assembly No. 4 indicate a rather poor calculation of the adjoint spectrum. The moderately poor agreement for the calculated and measured values for U^{238} in all assemblies cannot be entirely attributed to the inadequacy of the absorption or fission cross sections for this material, since the calculated value of the central U^{238}-to-U^{235} ratio is close to the measured value.

The assumed cross section for rhenium is some 25% higher than the measurements would indicate. This implies that the effect of rhenium has not been underestimated in proposed reactor core designs involving significant amounts of this material. Since this material was not in the 201 library, its cross section is given in the appendix.

A number of samples containing enriched isotopes of tungsten were made available by the Lewis Flight Laboratory. Sample weights, isotopic composition, and central-worth measurement results for these isotopes are shown in Table VIII. Differences between W and WO_3 measurements reported in Table VII and those in Table VIII (samples 5 and 0, respectively), are slightly larger than expected from the experimental errors involved for the conditions under which the experiment was performed.

TABLE VIII. Central Worths of Separated Tungsten Isotopes

Sample Identification Number:	Normal WO_2 0	Separated Metals 1	2	3	4	Normal Metal 5	W^{186} 6	$W^{184}O_3$ 7
Isotopic composition								
W^{182}	26.4	36.9	24.1	12.5	5.8	26.4	1.6	1.91
W^{183}	14.4	17.7	14.7	9.8	5.7	14.4	2.1	1.87
W^{184}	30.6	31.5	34.2	30.8	23.3	30.6	11.6	94.3
W^{186}	28.4	13.9	26.9	46.8	65.1	28.4	84.7	1.91
Weight, g	177.08	257.85	173.74	237.14	211.44	224.47	209.37	163.59
Central worths, Ih/kg								
Reference Assembly[a]	-2.7	-12.2	-11.0	-10.1	-8.3	-11.4	-7.0	-5.9
ZPR-6 Assembly No. 1	-24.1	-26.7	-24.5	-23.9	-21.7	-24.4	-20.7	-22.9
ZPR-6 Assembly No. 4	-13.7	-20.2	-18.7	-17.0	-14.7	-19.3	-13.1	-14.6

[a]ZPR-6 Assembly No. 2.

ZPR-6 Assembly No. 2 is the only other fast spectrum in which these samples are known to have been measured. These results and those obtained on the ZPR-9 assemblies are not easily compared since the "reference core" here is a large (650-liter) carbide core with approximately 36 v/o sodium. Its spectrum was quite soft relative to those of the ZPR-9 assemblies, as indicated by the following central worths: U^{235} = +104 Ih/kg, U^{238} = -6.2 Ih/kg, B^{10} = -1843 Ih/kg, C = +16.9 Ih/kg. Comparing normal tungsten to its oxide, we see that oxygen in the ZPR-9 assemblies has the same sign and about the same magnitude (-22.4 and +18.4 Ih/kg for Assemblies No. 1 and 4, respectively) as reported in Table VII. The equivalent oxygen worth in the reference assembly is +47.6 Ih/kg, consistent with the Al and Al_2O_3 differences and the positive worth of graphite.

4. Central Hydrogen Worths

Scattering by hydrogen of the real-flux spectrum in all but Assembly No. 4 is generally into a region of lesser adjoint flux, and the central hydrogen worth is therefore negative. Quantitative results are difficult to predict, both in sign and in magnitude.

The experimental program has been limited to central-worth measurements of hydrogenous materials as a function of sample size. Both powdered and solid Lucite, as well as solid polyethylene, have been used as samples. Corrections for oxygen and carbon in the samples have been made. Figure 8 shows the integral hydrogen worth as a function of sample size for Assemblies No. 3 and 4. The worth per gram as a function of sample size is also shown.

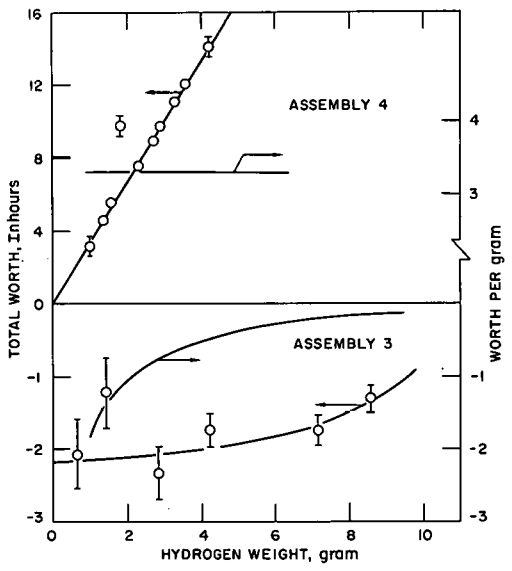

112-7909

Fig. 8. Central Hydrogen Worth in Assemblies No. 3 and 4

The high degree of the self-shielding in hydrogen is illustrated in Fig. 8 for Assembly No. 3. Quantitatively, this means that single and multiple scattered neutrons go into energy regions of approximately equal importance. The adjoint flux spectrum must be moderately constant through most of the region below the peak of the real flux spectrum. Contrarily, the adjoint flux spectrum in Assembly No. 3 appears to be increasing with decreasing energy. Very large samples (greater than about 11 g of hydrogen) may change the sign of the central worth in Assembly No. 3. Clearly, samples sufficiently large to effectively moderate the incident neutron-to-energy regions of large U^{235} fission probabilities will have a positive sign. There is the question of the applicability of perturbation theory to analysis for such large quantities of hydrogen, so that some caution must be exercised in interpreting such data.

5. Central Worths of Hydrogen-Boron Mixture

Most materials proposed as control elements in a fast reactor are not very black at the higher neutron energies. However, their control worth can be enhanced by the addition of moderating material, usually hydrogen. It is therefore of interest to measure the worth of various mixtures of hydrogen and boron and to determine the optimum weight ratios for maximum reactivity control.

Homogeneous mixtures of Lucite powder and amorphous boron were sealed in aluminum cans, and their central worths were determined

as a function of H:B weight ratios. Because of the different densities of the materials (Lucite powder, 0.4 g/cm^3; powdered boron, 0.6 g/cm^3; solid Lucite, 1.18 g/cm^3; amorphous boron, 2.34 g/cm^3), it was necessary to normalize the measured worths to unit mixture weights. The data taken from Assembly No. 4 measurements are shown in Fig. 9. From a smooth curve drawn through these points (curve A), the worth per gram of boron was determined and is shown as curve B. It appears that in the spectrum of Assembly No. 4, a 65:35 w/o mixture of Lucite:boron has the maximum negative worth per gram of boron.

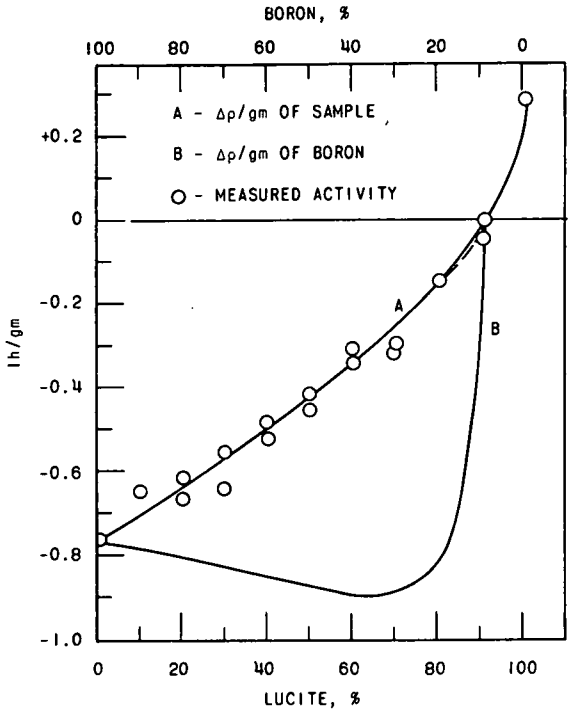

112-7842

Fig. 9. Central Worth of Boron-Lucite Mixtures in Assembly No. 4

6. Spatially Dependent Reaction Rates

Calculations of the real and adjoint flux spectra in the core center are moderately straightforward and have relatively small errors with regard to the application of diffusion theory and uncertainties in the aluminum cross sections. A more sensitive test of both the cross sections and the calculational model is the evaluation of the accuracy of the calculated spatially dependent reaction rates, particularly in the core-reflector region. In this region the transport properties of aluminum are most apparent, the use of diffusion theory is of greatest suspect, and the coupling between core and reflector is most sensitively measured.

For all the ZPR-9 cores, diffusion-theory fluxes were calculated in cylindrical geometry for 26 mesh points in the core and 15 in the reflector. Summing the products of these fluxes and the group-averaged fission cross sections for U^{235} and U^{238} over the 16 groups gives the reaction rates at each mesh point. The results are shown as the small triangles in Figs. 10 to 13 for Assemblies No. 1 through 4, respectively. The measured data are shown as the open boxes. All reaction rates are normalized to unity at the core center. The agreement between measured and calculated rates is very good, showing that the spatially dependent fluxes can be predicted with good accuracy.

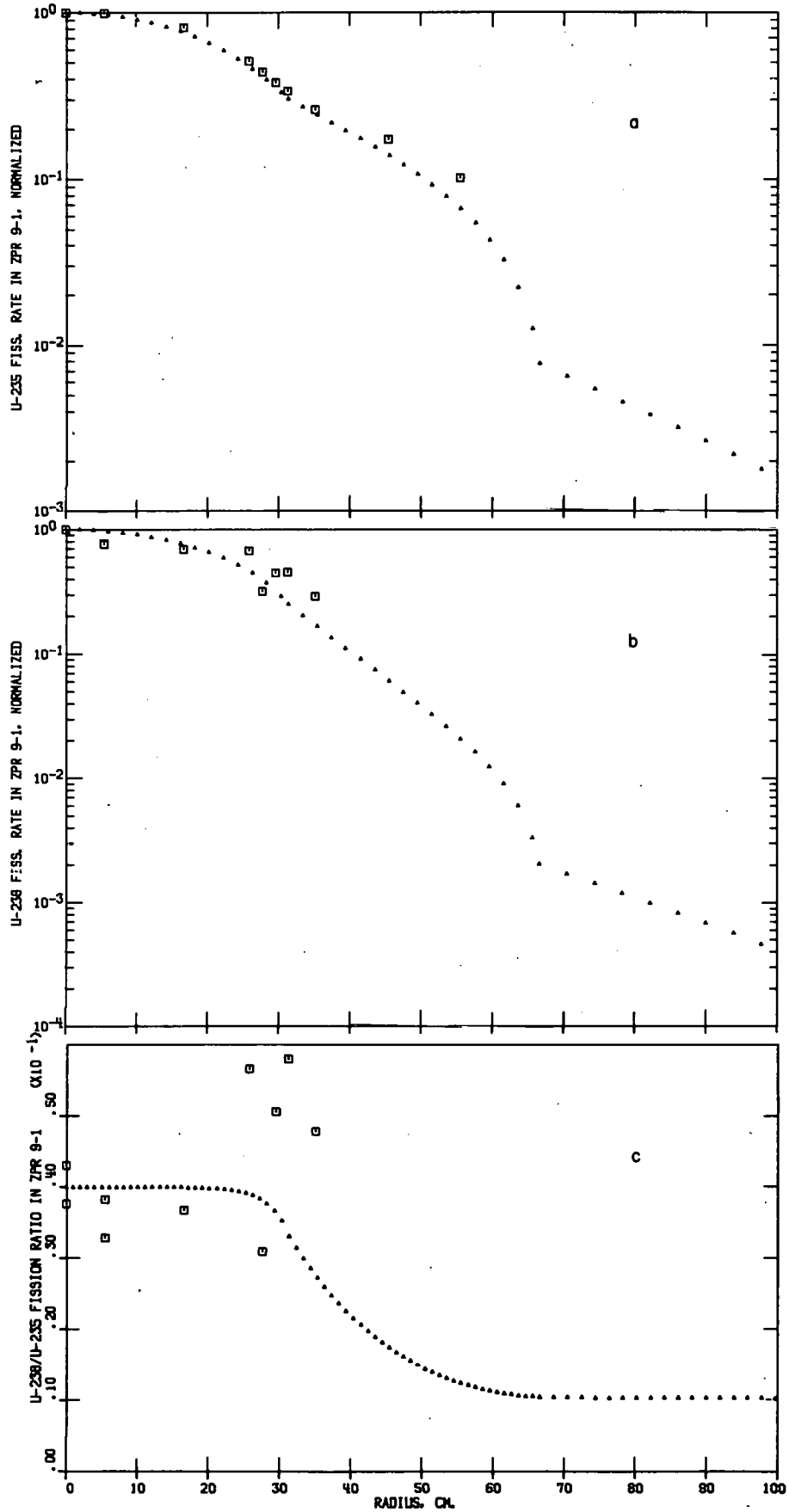

Fig. 10. U^{238} and U^{235} Space-dependent Fission Rates and Their Ratios in Assembly No. 1

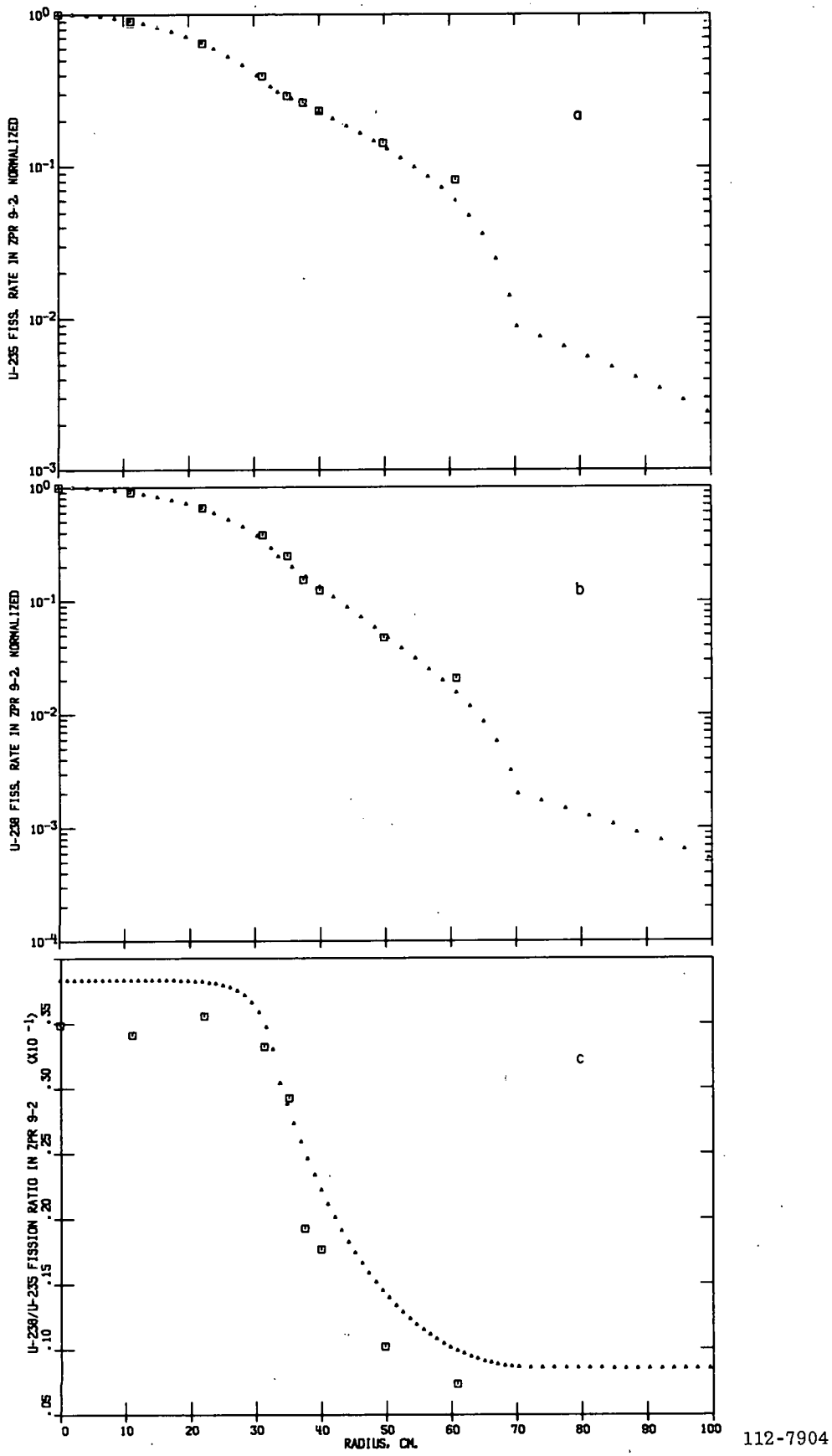

Fig. 11. U^{238} and U^{235} Space-dependent Fission Rates and Their Ratios in Assembly No. 2

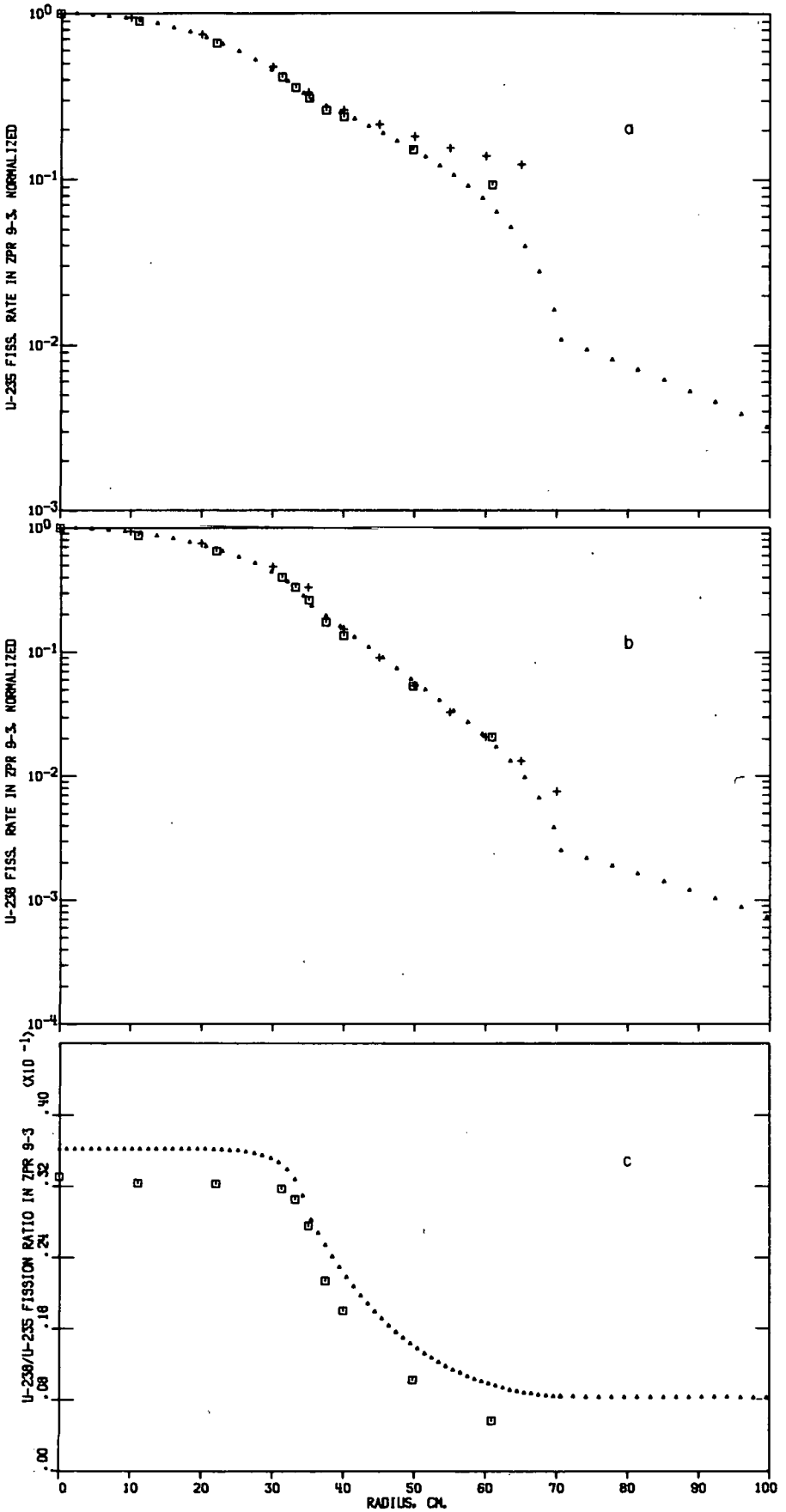

Fig. 12. U^{238} and U^{235} Space-dependent Fission Rates and Their Ratios in Assembly No. 3

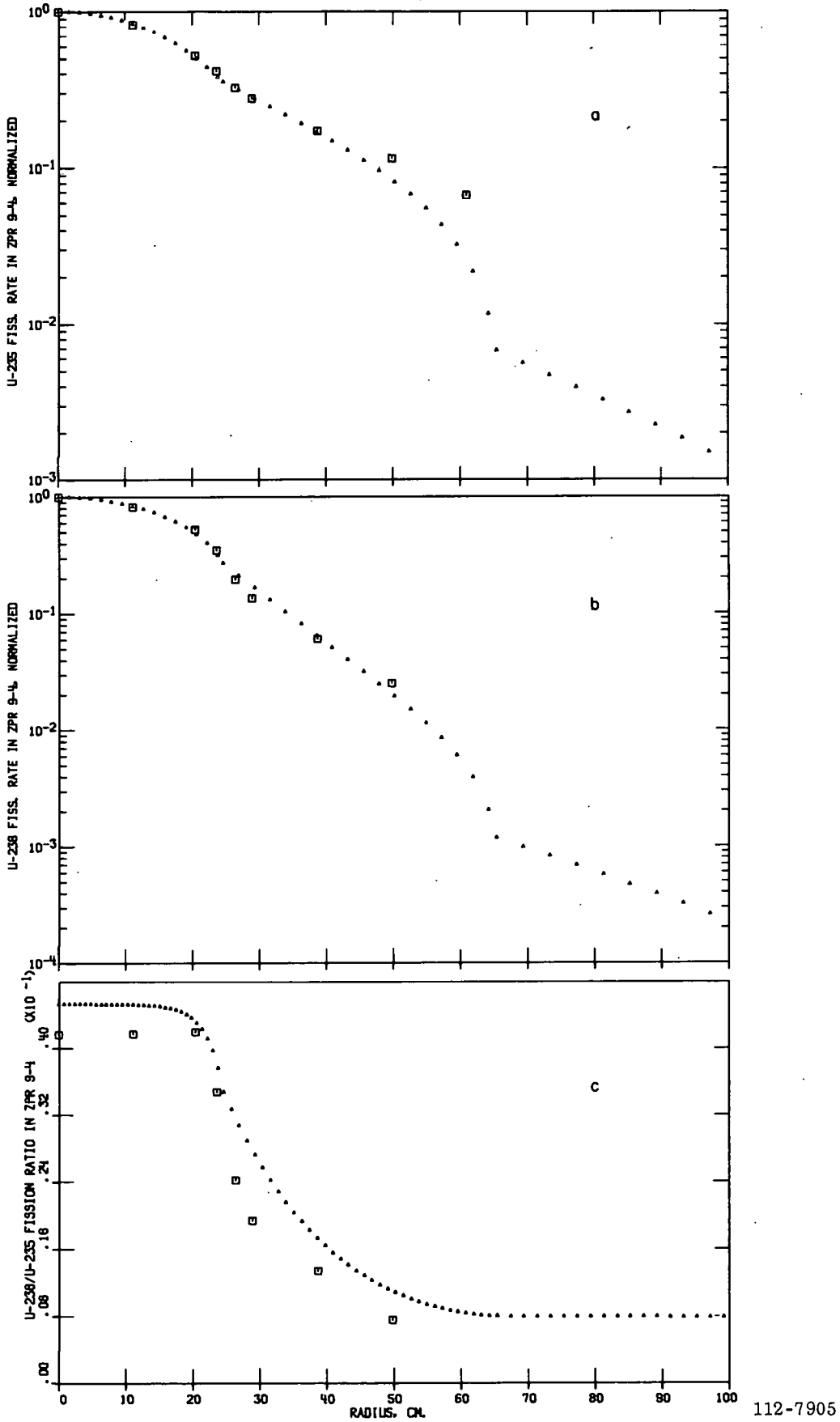

Fig. 13. U^{238} and U^{235} Space-dependent Fission Rates and Their Ratios in Assembly No. 4

The bottom curve in each figure is the spatially dependent ratio between U^{238} and U^{235} fissions. The calculated fission ratios are consistently about 10% higher than the experimentally determined value. This could be due to one of the following:

a. The U^{235} fission cross section is some 10% too low.

b. The U^{238} fission cross section is some 10% too high.

c. The calculated spectrum is too hard, putting a larger fraction of fissions above the U^{238} threshold.

Items a and c can be excluded on the basis of the much better agreement between the calculated and measured values of the central worths reported in Table VII, particularly for U^{235}. The calculated central worths for U^{238} are consistently 15-20% too negative, indicating either an overestimate of the absorption or an underestimate of the fission in U^{238}, the opposite indicated by b above. Further discussion is deferred to Section IV.B.

In addition to the foil data shown as the open squares, the fission distributions for U^{235}, U^{238}, Pu^{239}, and Np^{237} were measured with miniature solid-state detectors in Assembly No. 3. Results for the uranium isotope are shown as the + symbols in Fig. 12 and agree well with the foil data. Results for Pu^{239} and Np^{237} are shown in Figs. 14 and 15, respectively. No calculations are available for the Np^{237} since this isotope is not in the ANL 201 cross-section set.

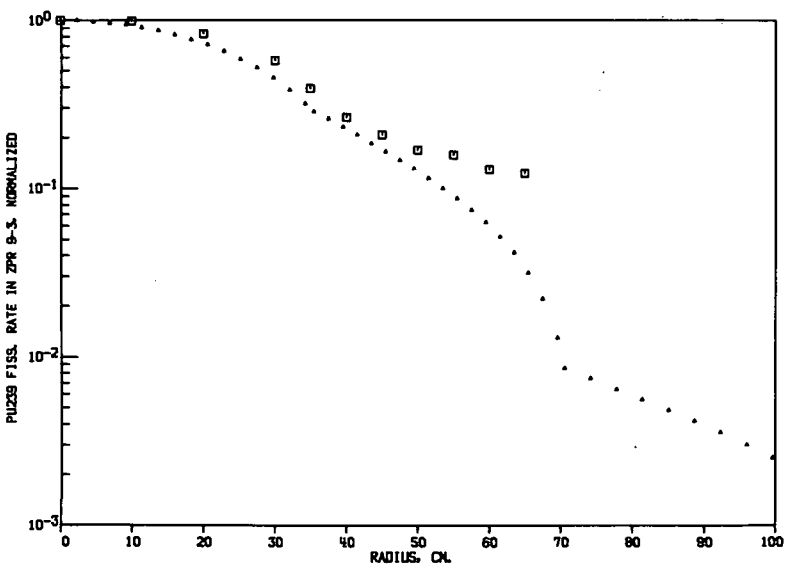

112-7911

Fig. 14. Pu^{239} Space-dependent Fission Rate in Assembly No. 3

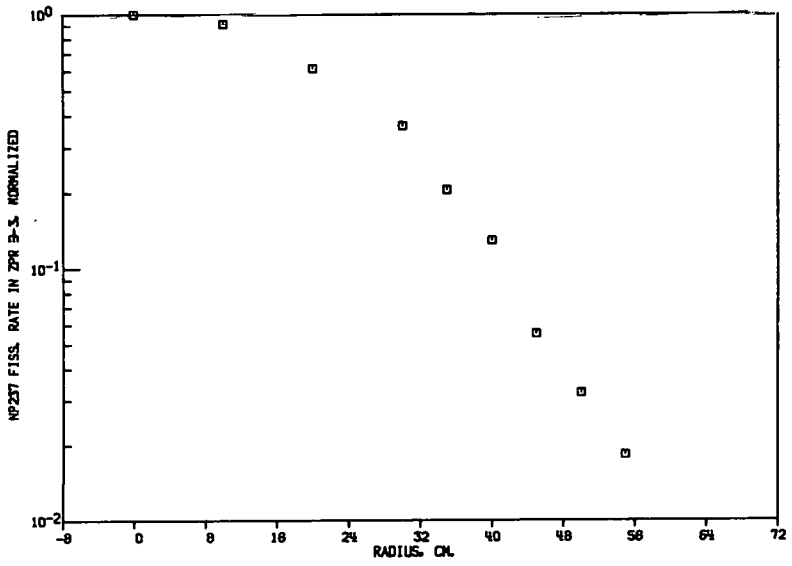

112-7910

Fig. 15. Np^{237} Space-dependent Fission Rate in Assembly No. 3

The boron capture rate was measured with a miniature BF_3 counter. The results are shown in Figs. 16 and 17 for Assemblies No. 3 and 4, respectively.

A single determination (in Assembly No. 4) was made of the spatially dependent U^{234} fission rate using the solid-state counter. This is shown in Fig. 18.

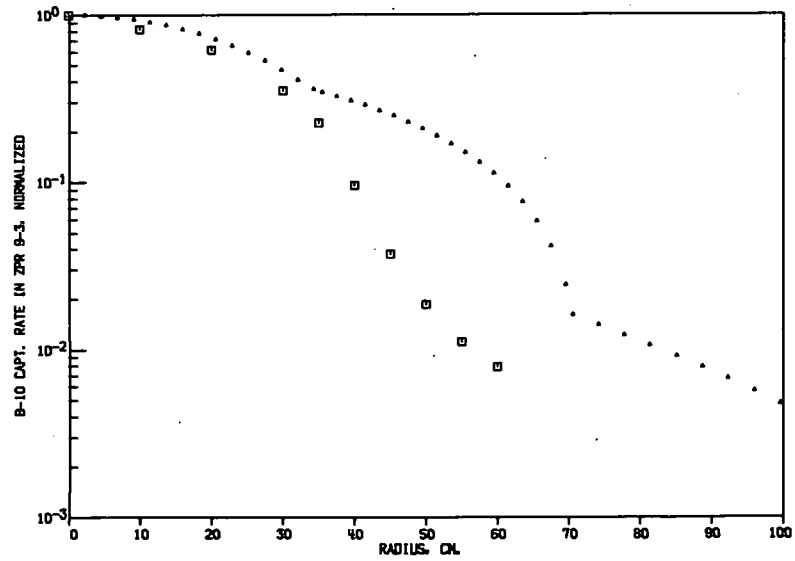

112-7913

Fig. 16. B^{10} (n,α) Space-dependent Fission Rate in Assembly No. 3

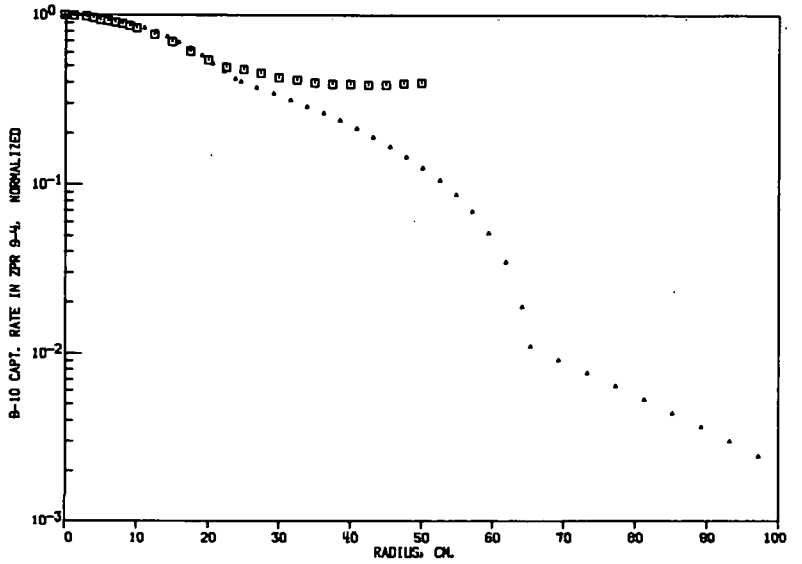

112-7914

Fig. 17

B^{10} (n,α) Space-dependent Fission Rate in Assembly No. 4

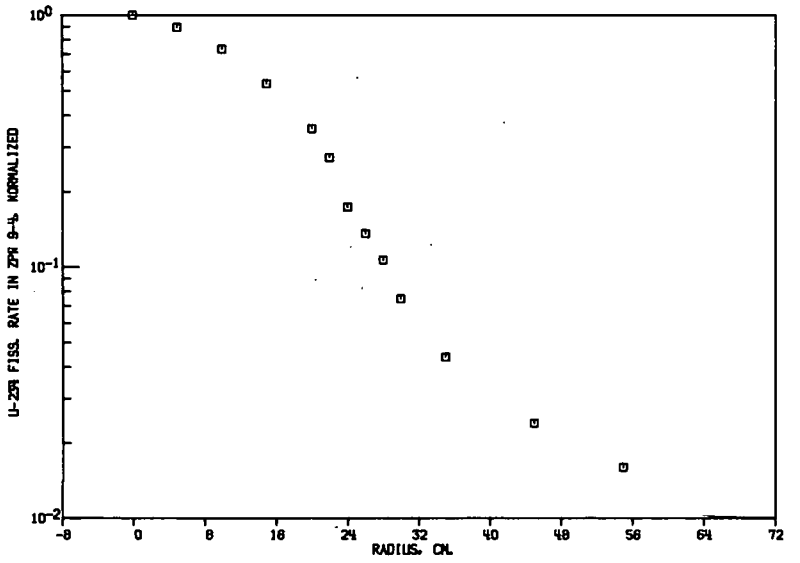

112-7912

Fig. 18

U^{234} Space-dependent Fission Rate in Assembly No. 4

C. Reflector Studies

Of the four assemblies studied, Assembly No. 4 had the highest fuel concentration and the smallest volume, and was thus the most sensitive to changes in the reflector. Perturbation calculations were performed for the spatial dependence of the reactivity for a scatterer (carbon), an absorber (rhenium), and tungsten because of its general interest to the program. The effects of these materials at the core-reflector interface is of special interest because of the vastly different asymptotic spectra in these two regions.

The experimental procedure was to install horizontal slabs of the material of interest above and below the radial surface of the core and over its full length. Reactivities were determined from calibrated control rods. Results of these measurements are given in Table IX with the geometry of

the experiment and the meanings of the variables indicated in Fig. 19. An effective mean radius was determined for each slab from the following expression:

$$\bar{r} = \frac{\int_{slab} r(x, y)\, dx\, dy}{\int_{slab} dx\, dy} = \frac{1}{WT} \int_{-W/2}^{+W/2} dx \int_{0}^{T} \sqrt{(d+y)^2 + x^2}\, dy,$$

where x and y are in the directions of W and T, respectively. The effective solid angle is then

$$\bar{\Omega} = 2 \tan^{-1} \frac{W/2}{\bar{r}} \text{ radians.}$$

TABLE IX. Reflector Replacement Worths

Aluminum Removed, kg	Material Added				$\bar{\Omega}$, radians	$\bar{r}$, cm	$\Delta\rho$, Relative to Aluminum, Ih	$\Delta\rho$/weight, Relative to Void, Ih/kg
	d, cm	W, cm	T, cm	Weight, kg				
				Aluminum (45% Density)				
11.430	24.89	16.59	2.54	4.984	1.26	26.59	-66.74	+10.35
11.430	27.65	16.59	2.54	4.984	1.19	29.31	-44.61	+6.92
38.101	35.95	27.65	5.08	16.613	1.79	31.89	-40.24	+1.87
53.341	41.48	38.71	5.08	23.258	1.76	45.41	-29.66	+0.99
				Carbon				
11.430	24.89	16.59	2.54	7.032	1.26	26.59	+45.55	+13.63
11.430	27.61	16.59	2.54	7.032	1.14	29.27	+37.87	+11.73
22.860	30.42	16.59	5.08	14.064	1.00	33.31	+65.21	+8.95
38.101	35.95	27.65	5.08	23.440	1.79	31.89	+93.14	+5.69
53.341	41.48	38.71	5.08	32.816	1.76	45.41	+98.03	+3.89
				Rhenium				
5.715	24.88	16.59	1.28	43.100	1.30	25.96	-133.48	-3.68
5.715	27.03	16.59	1.28	43.100	1.20	28.08	-72.12	-2.11
11.430	30.41	16.59	2.54	86.200	1.04	32.04	-71.72	-1.02
9.525	40.09	27.65	1.28	71.834	1.36	41.50	-23.21	-0.40
13.335	45.62	30.71	1.28	100.567	1.33	47.10	-7.88	-0.12

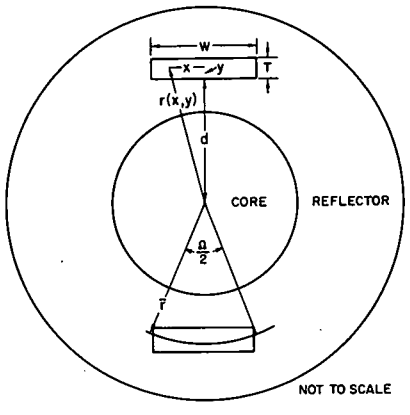

112-7921

Fig. 19

Geometry for Material Worths at Core Edge

IV. KINETICS

A. Introduction

The prompt-neutron lifetime in fast reactors is not only important for safety analyses, but it provides a sensitive index for the neutron spectrum. Such an index can be quite valuable in cross-section set diagnostics. Therefore, it is essential that a meaningful comparison be made between the calculated prompt-neutron lifetimes and those inferred from measurements. It has been known for some time[4-6] that the calculated prompt-neutron lifetime, ℓ, in a fast reactor is shorter than the lifetime obtained through the Rossi-alpha measurement. Davey[4] reports that, on the average, ℓ is 1.34 times the experimental value. Brunson et al.[5] estimate the uncertainty in β_{eff} to be about 5% and the uncertainty in the experimental Rossi-alpha to be about another 5%. At worst, then, the inherent uncertainty in ℓ is less than 10%. Thus, the discrepancy between the measured and calculated values of ℓ is outside the uncertainties associated with either α or β_{eff}. Without further systematic study, it is not known whether the calculation, the measurement, or both, are in error.

B. Areas for Investigation

The heterogeneity effects on the neutron spectrum and hence on the prompt-neutron lifetime were studied by Meneghetti and Loomis,[7] and their conclusion, which is supported by experimental data, is that these effects are positive in $\Delta k/k$ (with a tendency to harden the spectrum and decrease the prompt-neutron lifetime).

Results of one-dimensional, multigroup, diffusion-theory studies of reflectors are ambiguous. The worth of a reflector in a static problem can be estimated with reasonable accuracy, but it is not clear what happens dynamically. More experimental work is needed in this area. Specifically, experiments designed to study the effects of reflector thickness as well as reflector material on the system are desirable. Such studies could lead to the determination of the origin of the fast-decaying modes of the prompt-neutron chains and their effects. Observations on ZPR-9 (Ref. 8) do not indicate if these modes are characteristic of the reflector or other transport phenomena. Such a study could also establish or reject the validity of the simple, one-group, two-region model discussed in Ref. 8. Parametric study of the decay rates of the prompt-neutron chains, as predicted by the one-group, two-region model, can be used as a guide for designing experiments. Results of this study are shown in Fig. 20, where α_2, the Rossi-alpha, and α_1, the fast-decaying mode, are plotted as a function of the worth of the reflector. In Fig. 20, ℓ_c and ℓ_r are the average lifetimes of the prompt neutron in the core and in the reflector, respectively. The α_2 decreases as the worth of the reflector is increased and also as the ratio ℓ_r/ℓ_c is increased. It is also seen from Fig. 20 that α_1 increases as the worth of the reflector is increased and decreases as the ratio ℓ_r/ℓ_c is increased.

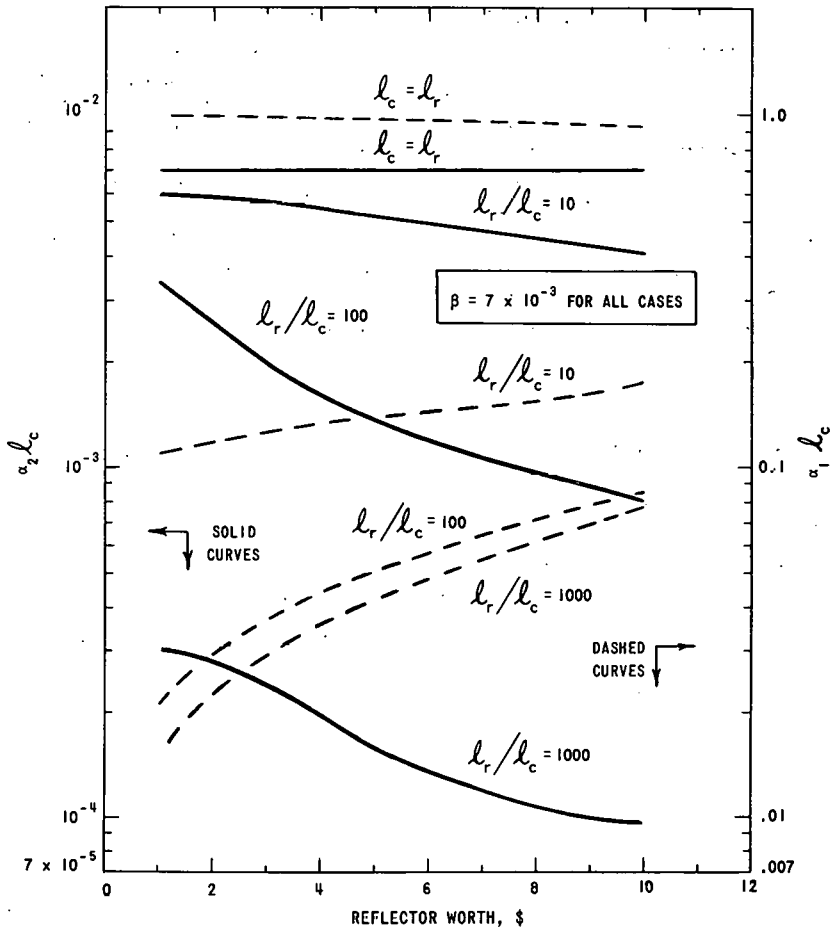

112-4717 Rev. 1

Fig. 20. One-group, Two-region Analysis of Prompt-decay Constant

The accounting of the neutrons in diffusion theory is also subject to question. For example, the leakage term is usually defined as $-\nabla \cdot J$, where J is the neutron current. However, in the derivation of the expression for J(r), it is assumed that the medium is infinite about r, has no sources of neutrons, and does not absorb neutrons. None of these assumptions is valid in fast reactors.

C. Comparison between Measurement and Calculation

Table X compares the measured and calculated prompt-neutron lifetimes for the first four assemblies of ZPR-9. The calculated values listed in Table X were obtained with the 201 cross-section set and one-dimension diffusion code. The discrepancies between the calculated and measured values of the prompt-neutron lifetimes are of the same magnitude as the discrepancies reported by Davey,[4] who used cross-section set ANL 634 (modified YOM set) and one-dimensional transport code.[10] The agreement in the discrepancies between Davey's results and the results reported here can be fortuitous since the cross-section sets and the codes used in the two cases are different.

TABLE X. Kinetic Parameters

	Reference Assembly[a]	ZPR-9 Assemblies			
		No. 1	No. 2	No. 3	No. 4
β_{eff} (calc)[b]	0.00725	0.00728	0.00723	0.00708	0.00664
Rossi-alpha (meas), $sec^{-1} \times 10^{-4}$	10.0	8.67	6.9	6.57	5.19
Prompt lifetime (exp), nsec	72.5	84.0	105.0	107.0	128.0
Prompt lifetime (calc), nsec[b]	64.9	60.5	73.9	81.7	95.0
(Exp - calc)/calc	0.11	0.38	0.42	0.30	0.34

[a]ZPR-6 Assembly No. 6.
[b]Calculated from a point-model reactor.

Good agreement between the calculated and measured values of the prompt-neutron lifetimes in small bare assemblies have been reported on Godiva[11] and other metallic U^{235} and Pu^{239} assemblies.[12] The cross-section sets used on these assemblies were not stated. It is not known whether the size of the core, the cross-section set, the fact that the core was bare, the method of calculation, or any combination of these is responsible for this agreement.

APPENDIX

Cross Sections Employed in Study

The present study employed a familiar and widely used cross-section set[13] which was supplemented by some additional nuclide cross sections required in the study but not present in the original set. Only the cross sections for these additional materials, that is, for tungsten, rhenium, and B^{10}, will be described.

A. Tungsten Cross Sections

One of the initial analytical tasks in the study of rocket reactors at Argonne was the evaluation of available microscopic data for tungsten and the generation of tungsten cross sections. Actually the study resulted in the generation of a number of tungsten cross-section sets that differed in various details such as spectra over which the cross sections were averaged, averaging methods, and the basic microscopic data used. The methods employed and the data sources used are presented in Ref. 14. Subsequently, the generated cross-section sets were subjected to a range of experiment-to-calculation comparisons.[15] The purpose of the comparisons was to evaluate the sensitivity of various calculated reactor parameters to differences in the tungsten cross-section sets and to determine which of the sets had the highest degree of theory-to-experiment agreement. For the type of reactor neutron spectra considered in this study, the cross-section set shown in Table XI was very satisfactory. The properties of assemblies containing up to 70 v/o of tungsten were calculated within the known limitations of the calculational methods used, and no

TABLE XI. Natural Tungsten Cross-section Set

Energy Group, j	$\sigma_{n,r}$	σ_{REM}	σ_{TR}	$\sigma_{j\to j}$	$\sigma_{j\to j+1}$	$\sigma_{j\to j+2}$	$\sigma_{j\to j+3}$	$\sigma_{j\to j+4}$	$\sigma_{j\to j+5}$
1	0.026	2.478	4.562	3.657	1.262	0.33	0.54	0.28	0.04
2	0.072	2.476	4.625	4.512	1.004	0.99	0.36	0.05	
3	0.10	1.468	4.379	5.051	0.878	0.39	0.08	0.02	
4	0.09	0.554	4.626	6.042	0.444	0.02			
5	0.13	0.308	6.641	7.62	0.178				
6	0.263	0.309	9.617	9.828	0.046				
7	0.651	0.750	12.838	12.242	0.099				
8	1.824	1.926	15.170	13.292	0.102				
9	3.238	3.345	17.812	14.520	0.107				
10	0.645	0.728	13.489	12.807	0.083				
11	8.359	8.759	41.564	32.925	0.400				
12	7.745	7.921	13.871	5.972	0.176				
13	3.101	3.185	8.409	5.243	0.084				
14	3.741	3.810	9.237	5.447	0.069				
15	7.326	7.542	12.890	5.367	0.0216				
16	14.412	14.412	20.00	5.607					

systematic error could be assigned to the tungsten cross sections. The mean neutron energy of these assemblies is 0.2 MeV; thus any self-shielding in the tungsten resonances is not important. The cross-section set can be used successfully also for significantly softer neutron spectra if the tungsten concentration does not exceed 20%. For higher tungsten concentrations, the self-shielding built into the capture cross sections of the resonance region is not sufficient, and the cross sections below 500 eV should be re-evaluated.

B. Rhenium Cross Sections

Rhenium has the potential of becoming important in the nuclear-rocket field as an alloying material that imparts better working properties to the very difficultly machined tungsten. Neutronically, it is rather undesirable material because of its large capture cross section. If it is to be used at all, it can be used only in fast-spectrum reactors and even then preferably at low concentrations.

The large capture cross section does, however, suggest that rhenium could be used as a control material. Its volumetric absorption is equal to that of natural boron in most spectra. In other aspects; i.e., on a weight or cost basis, rhenium is inferior to boron; thus it would be used only if structural or n,α reaction heating problems made the use of boron impossible.

Basic microscopic data for rhenium are presently quite incomplete especially as far as the inelastic scattering levels are concerned. Accordingly, an interim rhenium cross-section set was constructed which uses newly available rhenium capture data[16] but borrows the inelastic scattering matrix from tungsten. In the present study, this limitation did not cause any difficulty since, as a core material, rhenium is invariably used at a fairly low concentration.

This interim rhenium cross-section set is shown in Table XII. The set should not be used for problems in which rhenium makes up more than 10% of the core composition.

C. Boron-10 Isotope Cross Sections

The B^{10} cross sections were generated by increasing the capture cross section of the natural boron set given in Ref. 13 by a factor of 5 and by adjusting the σ_{TR} and σ_{REM} reaction cross sections accordingly. The resulting cross-section set is shown in Table XIII.

Some past studies[4] have indicated that the boron capture rate is difficult to estimate correctly in fast-reactor spectra. For example, in the

study of Ref. 4, the central worth coefficient of boron, which is almost entirely determined by the capture reaction, was consistently underestimated in comparison with the experimental values by ~30%. Since the capture cross section of boron itself is one of the best known cross sections, the fault lies in the calculation of the neutron spectrum. Such a consistent error would be inconvenient in the present study; thus pains were taken to explore the accuracy with which the cross-section set used in this report computes the boron reaction rate. It was determined that in quite a wide range of spectra the cross-section set presented in Table XIII predicts the central B^{10} reactivity worth within 5-10% of the experimental value.

TABLE XII. Rhenium Cross-section Set

Energy Group, j	$\sigma_{n,r}$	σ_{REM}	σ_{TR}	$\sigma_{j\to j}$	$\sigma_{j\to j+1}$	$\sigma_{j\to j+2}$	$\sigma_{j\to j+3}$	$\sigma_{j\to j+4}$	$\sigma_{j\to j+5}$
1	0.11	2.563	4.059	3.657	1.263	0.33	0.54	0.28	0.04
2	0.18	2.584	4.452	4.512	1.004	0.99	0.36	0.05	
3	0.25	1.618	3.946	5.051	0.878	0.39	0.08	0.02	
4	0.33	0.794	4.437	6.042	0.444	0.02			
5	0.68	0.818	7.120	7.62	0.178				
6	1.4	1.445	10.752	9.828	0.045				
7	3.16	3.259	15.340	12.242	0.099				
8	8.16	8.262	21.554	13.292	0.102				
9	34.2	34.307	48.83	14.520	0.107				
10	5.645	5.728	18.53	12.807	0.083				
11	8.359	8.759	41.68	32.925	0.40				
12	7.745	7.921	13.89	5.972	0.176				
13	3.101	3.185	8.43	5.243	0.084				
14	3.741	3.81	9.26	5.447	0.069				
15	7.326	7.542	12.91	5.367	0.216				
16	14.412	14.412	20.02	5.607	-				

TABLE XIII. B^{10} Isotope Cross-section Set

Energy Group, j	$\sigma_{n,r}$	σ_{REM}	σ_{TR}	$\sigma_{j\to j}$	$\sigma_{j\to j+1}$	$\sigma_{j\to j+2}$	$\sigma_{j\to j+3}$	$\sigma_{j\to j+4}$	$\sigma_{j\to j+5}$
1	0.20	0.87	1.68	0.81	0.67				
2	0.30	0.72	2.03	1.31	0.42				
3	0.20	1.08	2.30	1.22	0.88				
4	0.40	0.90	2.59	1.69	0.50				
5	1.35	1.73	4.24	2.51	0.38				
6	3.05	3.41	6.52	3.11	0.36				
7	7.50	7.87	10.97	3.1	0.37				
8	17.00	17.38	20.47	3.09	0.38				
9	40.0	40.38	43.47	3.09	0.38				
10	82.0	82.53	85.47	2.94	0.53				
11	145.0	145.58	148.47	2.89	0.58				
12	260.0	260.53	263.47	2.94	0.53				
13	460.0	460.58	463.47	2.89	0.58				
14	755.0	755.7	758.47	2.77	0.70				
15	1365.	1365.46	1368.47	3.01	0.46				
16	3346.5	3346.5	3349.97	3.47	-				

REFERENCES

1. R. K. Long *et al.*, *Fast Neutron Power Reactor Studies in ZPR-III*, Peaceful Uses of Atomic Energy *12*, Reactor Physics, United Nations, Geneva, 119 (1958).
2. W. Y. Kato, G. J. Fischer, and L. R. Dates, *Safety Analysis Report Argonne Fast Critical Facility (ZPR-VI)*, ANL-6271 (Dec 1963).
3. *Reactor Development Program Progress Report*, ANL-6880, 10 (March 1964).
4. W. G. Davey, *An Analysis of 23 ZPR-III Fast Reactor Critical Experiments*, Nucl. Sci. Eng. *19*, 259 (1964).
5. D. Meneghetti, *Recent Advances and Problems in Theoretical Analyses of ZPR-III Fast Critical Assemblies*, Physics of Fast and Intermediate Reactors *1*, 457-487, International Atomic Energy Agency, Vienna (1962).
6. G. S. Brunson, R. N. Curran, J. M. Gasidlo, and R. J. Huber, *A Survey of Prompt-neutron Lifetimes in Fast Critical Systems*, ANL-6681 (Aug 1963).
7. D. Meneghetti and M. F. Loomis, *Calculation of Heterogeneity Effects in ZPR-III Fast Assemblies Using the DSN Programs*, ANL-6218 (Nov 1960).
8. R. A. Karam, *Measurement of Rossi-Alpha in Reflected Reactors*, Trans. Am. Nucl. Soc. *7*, No. 2, 282 (Nov 1964).
9. D. Meneghetti, *Introductory Fast Reactor Physics Analysis*, ANL-6809 (Dec 1963).
10. B. G. Carlson, *Numerical Solution of Transient and Steady State Neutron Transport Theory Problems*, LA-2260 (1959).
11. T. Asaoka *et al.*, *Prompt Neutron Lifetime Calculations in Fast Assemblies*, Trans. Am. Nucl. Soc. *7*, No. 2, 514 (Nov 1964).
12. G. E. Hansen, *Status of Computational and Experiment Correlations for Los Alamos Fast-neutron Critical Assemblies*, Proc. of the Seminar on the Physics of Fast and Intermediate Reactors, Sponsored by the International Atomic Energy Agency *1*, 445-455, Vienna (1962).
13. G. E. Hansen and W. H. Roach, *Six and Sixteen Group Cross Sections for Fast and Intermediate Critical Assemblies*, LAMS-2543 (1961).
14. R. Kaiser and W. B. Loewenstein, "Natural Tungsten Cross Sections for Fast and Intermediate Neutron Spectra," *Reactor Physics Division Annual Report, July 1, 1963 to June 30, 1964*, ANL-7010, 129-131 (Jan 1965).
15. K. Almenas, "Verification of Tungsten Cross Sections," ibid., 131-134.
16. D. C. Stupegia, M. Schmidt, and A. A. Madson, *Fast Neutron Capture in Rhenium*, to be published in J. Nucl. Eng. (Reactor Science and Technology).
17. *Reactor Physics Constants*, ANL-5800, Second Edition (July 1963).
18. The RP-122 code is an updated version of AIM-6 (H. P. Flatt and D. C. Balder, *The AIM-6 Code*, NAA Program Description, Jan 1961).